Chemosphere 250 (2020) 126325

Contents lists available at ScienceDirect

Chemosphere

journal homepage: www.elsevier.com/locate/chemosphere

Beyond carbon capture towards resource recovery and utilization: fluidized-bed homogeneous granulation of calcium carbonate from captured CO_2

Yao-Hui Huang [a], Sergi Garcia-Segura [b], Mark Daniel G. de Luna [c, d, *], Arianne S. Sioson [c], Ming-Chun Lu [e, **]

[a] Department of Chemical Engineering, National Cheng Kung University, Tainan, 70101, Taiwan, ROC
[b] Nanosystems Engineering Research Center for Nanotechnology-Enabled Water Treatment, School of Sustainable Engineering and the Built Environment, Arizona State University, Tempe, AZ, 85287-3005, United States
[c] Environmental Engineering Program, National Graduate School of Engineering, University of the Philippines, Diliman, Quezon City, 1101, Philippines
[d] Department of Chemical Engineering, University of the Philippines, Diliman, Quezon City, 1101, Philippines
[e] Department of Environmental Resources Management, Chia Nan University of Pharmacy and Science, Tainan, 71710, Taiwan, ROC

HIGHLIGHTS

- Carbon dioxide was recovered by calcium carbonate granulation.
- Calcium carbonate removal and granulation efficiencies exceeded 95%.
- Effects of supersaturation and cross-sectional loading on granulation were examined.
- Physic-chemical characteristics of the recovered granules were analyzed.

GRAPHICAL ABSTRACT

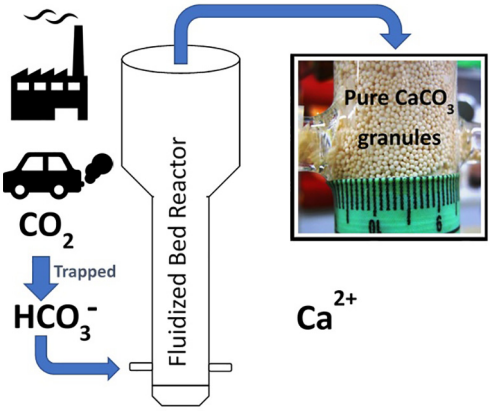

ARTICLE INFO

Article history:
Received 12 January 2020
Received in revised form
15 February 2020
Accepted 23 February 2020
Available online 26 February 2020

Handling Editor: Veeriah (Jega) Jegatheesan

ABSTRACT

Atmospheric carbon dioxide (CO_2) imbalance due to anthropogenic emissions has direct impact in climate change. Recent advancements in the mitigation of industrial CO_2 emissions have been brought about by a paradigm shift from mere CO_2 capture onto various adsorbents to CO_2 conversion into high value products. The present study proposes a system which involves the conversion of CO_2 into high purity, low moisture, compact and large $CaCO_3$ solids through homogeneous granulation in a fluidized-bed reactor (FBR). In the present study, synthetic solutions of potassium carbonate (K_2CO_3) and calcium hydroxide ($Ca(OH)_2$) were used as sources of carbonate and precipitant, respectively. The effects of the degree of supersaturation (S) as chemical loading and influx flow rate (Q_T) as hydraulic loading on $CaCO_3$ granulation efficiency were investigated. In the study, S was varied from 10.2 to 10.8 and Q_T from 40 to

* Corresponding author. Environmental Engineering Program, National Graduate School of Engineering, University of the Philippines, Diliman, Quezon City, 1101, Philippines.
** Corresponding author.
E-mail addresses: mgdeluna@up.edu.ph (M.D.G. de Luna), mmclu@mail.cnu.edu.tw (M.-C. Lu).

https://doi.org/10.1016/j.chemosphere.2020.126325
0045-6535/

Keywords:
Carbonate influent
Climate change
Fluidized-bed reactor
Granule characteristics
Influx flow rate

80 mL min^{-1} while the operating pH and calcium-is-to-carbonate molar ratio ($[Ca^{2+}]/[CO_3^{2-}]$) were set at 10 ± 0.2 and 1.50, respectively. Results showed that carbonate ions end product distribution had a highest carbonate granulation efficiency at $[Carbonate]_G$ of 95–96% using S of 10.6 and Q_T of 60 mL min^{-1}. Characterization of the granules confirmed high purity calcium carbonate. Overall, the transformation of industrial CO_2 emissions into a valuable solid product can be a significant move towards the mitigation of climate change from anthropogenic emissions.

1. Introduction

Atmospheric carbon dioxide (CO_2) imbalance due to anthropogenic emissions has direct impact in climate change. Current anthropogenic activities are associated to the emission of over 40 Gt of CO_2 annually due to the reliance on fossil fuels as energy source. Carbon dioxide (CO_2) emissions from industrial processes are the major contributors to the increasing global greenhouse gas emissions, accounting to 78% (Zhang and Huisingh, 2017). These greenhouse gas emissions have been associated to warming of atmosphere and oceans, losing of mass of the polar ice sheets, changing weather patterns, and rising sea levels (Moreira and Pires, 2016). If there would be no action taken, the current CO_2 atmospheric concentration of 409 ppm, would be expected to get doubled by 2050 reaching the point of no return (Singh et al., 2018).

Efforts have been made to reduce CO_2 emissions including shift to renewable energy sources, application of energy saving measures. However, the actual CO_2 level reduction is dependent upon to carbon capture and storage (CCS) technologies (Patricio et al., 2017). Capturing the CO_2 post-combustion emissions from major CO_2 emitting industries is a good option to control the atmospheric CO_2 concentration (Minelli et al., 2018; Thompson et al., 2018). CCS technologies discovered are vital means of preventing the industrial CO_2 emissions from being released in the atmosphere, however these are just short to intermediate-term solutions (Cheng et al., 2018; Wang et al., 2015). Currently applied CO_2 capture methods are mostly based in adsorption. These methods rely in CO_2 adsorption membranes in passive systems by considering post-combustion, pre-combustion and oxy-fuel combustion where captured CO_2 is stored by geo-sequestration consisting of CO_2 injection into underground geological formations (Khalilpour et al., 2015; Mukherjee et al., 2019; Sharma, 2018). Remediation approaches should go beyond simple storage by producing a market product. Revalorization of CO_2 by producing useful chemicals (e.g., methanol, formic, etc.) by artificial photosynthesis or electrochemical reduction are still under development (El-Khouly et al., 2017; Sánchez-Sánchez et al., 2012; Zhang et al., 2019). In this frame, Fluidized-bed Homogeneous Granulation (FBHG) process emerges as promising alternative. FBHG can produce pure granules $CaCO_3$ from CO_2 enriched solutions produced as result of conventional CO_2 capture. Proposed FBHG has been barely explored as carbon dioxide revalorization method, here we study its applicability as alternative method for calcium carbonate revalorization as chemical widely used in industrial applications, health/dietary applications, and agricultural use. FBHG process has a continuous system that will not just capture and store CO_2 but converts it into useful product. The advantages of using fluidized-bed granulation process are good mixing, high purity, bigger size granules produced, and less chemicals requirement (Salcedo et al., 2016; Chen et al., 2015).

Fig. 1 shows the schematic flow of the CO_2 emission reduction proposed. The CO_2 gas would be captured using higher equimolar amount of KOH solution as absorbent and resulting K_2CO_3 solution would be used as feedstock to granulate $CaCO_3$ as presented in Eqs. (1)–(3). KOH solution as chemical absorbent has a high efficiency with absorption capacity of 19.36–23.33 g L^{-1} at 0.5–1 M KOH concentration (Smirnova et al., 2014; Medinsky, 1986; Yoo et al., 2012). Note that similar effects can be observed using NaOH instead. Therefore, the selection of the base can be conducted in function of capital expenditures based on market price.

$$KOH(aq) + CO_2(g) \leftrightharpoons KHCO_3(aq) \quad (1)$$

$$KHCO_3 + KOH \leftrightharpoons K_2CO_3 + H_2O \quad (2)$$

$$K_2CO_3 + Ca(OH)_2 \leftrightharpoons CaCO_3(s) + 2KOH \quad (3)$$

The K_2CO_3 solution as the product from the chemical absorption will then enter the FBR as reactant with $Ca(OH)_2$ solution as precipitant to form $CaCO_3$ granules as the final product. The KOH solution as by-product of FBHG process will be recycled back to the absorbent column. This study aims to evaluate the capabilities of FBHG technologies applied in the context of carbon capture and utilization. The best operating conditions of supersaturation (S) and influx flow rate (Q_T) that would obtain highest carbonate granulation efficiency, lowest carbonate effluent residues, and least carbonate fines fraction was determined. Moreover, the surface morphology and chemical characteristics of the biggest granules produced by the FBR was investigated in terms of its molecular, structural and elemental composition.

2. Materials and methods

2.1. Chemicals

Chemicals and reagents used were of analytical grade with no further purification. Synthetic K_2CO_3 and $Ca(OH)_2$ solutions, as influent carbonate and precipitant calcium sources, respectively, were prepared by dissolving separately the K_2CO_3 (99.5%, New Star Instrument, Taiwan) and $Ca(OH)_2$ (90%, New Star Instrument, Taiwan) in reverse osmosis (RO) water from the RODA ultrapure water system (resistance of 18.2 MΩ) with their specified concentrations. These solutions emulate the concentrations and conditions of CO_2 saturated solutions of CCS devices. The solution pH of the calcium hydroxide solutions were set at 8 ± 0.05 while the

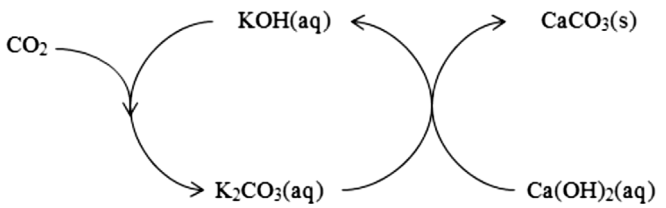

Fig. 1. Schematic diagram of the CO_2 emission reduction through KOH absorption and $CaCO_3$ granulation.

potassium carbonate solutions were set at operating pH of 10 ± 0.2 using sodium hydroxide (NaOH, Formosa Plastic Corporation, Taiwan) and nitric acid (70% HNO_3, New Star Instrument, Taiwan). Reagents used for alkalinity test were N/50 sulfuric acid (95–98% H_2SO_4, Panreac AppliChem) as a titrant, 1% phenolphthalein solution (Phenolphthalein, New Star Instrument, Taiwan) as an indicator for phenolphthalein alkalinity, and 0.1% methyl orange (Methyl orange, Riedel-de Haën) as an indicator for total alkalinity.

2.2. Fluidized-bed reactor

The calcium carbonate precipitation by granulation were conducted in a cylindrical Pyrex glass fluidized-bed reactor (FBR) with total volume of 550 mL. The reactor design and configuration has been already optimized in previous works (Caddarao et al., 2018; Salcedo et al., 2016). The FBR reactor was divided into two defined regions divided by the lower and upper sections. The lower part which was the reaction region had dimensions of 80 cm in height and 2 cm in inner diameter. The region were granulation occurred had three inlets in the bottom section. The two horizontal inlets were for the reactant and precipitant, while the vertical inlet was for effluent recirculation. The glass beads inside the reactor supported the granulation bed to avoid bubble formation and clogging. Furthermore, glass beads acted as turbulence promotors allowing to distribute uniformly the liquid solution flow inside the reactor from the three inlets. The upper part which was the effluent region had dimensions of 15 cm in height and 4 cm in inner diameter. The sudden expansion decreased up flow velocity, thus preventing fine particles to be drained out.

2.3. Granulation experiments

Supersaturation (S) and influx flow rate (Q_T) were essential and critical factors that influenced the granulation. S is the state of a solution that promotes granulation, while Q_T is the sum of the reactant and precipitant flow rates that passes through a system (Chen et al., 2015). S or saturation index is commonly expressed as concentration of reactant as a function of solubility with formula given in Eq. (4), where IAP is the ion activity product, $[Ca^{2+}]$ represents the molar concentration of calcium ions, $[CO_3^{2-}]$ represents the molar concentration of carbonate, and K_{sp} is the solubility product constant. In granulation of $CaCO_3$ through FBHG process, it is important to check the degree of saturation in order to determine if the conditions would induce granulation.

$$S = \log\left(\frac{IAP}{K_{sp}}\right) = \log\frac{\left[Ca^{2+}\right]\left[CO_3^{2-}\right]}{K_{sp}} \quad (4)$$

In order to investigate the breakthrough of CO_2 emission capture and granulation by FBHG process, this paper aims to granulate carbonate from a synthetic solution through FBHG process by chemical reaction with a precipitant to produce $CaCO_3$ granules of new product. The reactor was initially loaded with glass beads of the same size up to 1 cm above the horizontal inlets which would help distribute uniformly the hydraulic loading and then filled with 450 mL RO water from the RODA ultrapure water system (resistance of 18.2 MΩ) up to the effluent outlet to avoid bubbling. Precipitation of calcium carbonate into granules was initiated by controlling the parameters, operating pH to 10 ± 0.2 and $[Ca^{2+}]/[CO_3^{2-}]$ to 1.50, and varying S to 10.2–10.8, and Q_T to 40–80 mL min^{-1}. The pH was defined to ensure available carbonate without leading to calcium hydroxide precipitation (a relatively insoluble species with $K_{sp} = 5.5 \times 10^{-6}$). The molar ratio $[Ca^{2+}]/[CO_3^{2-}]$ to 1.50 relies on the use of a surplus of calcium concentration to ensure complete removal of targeted CO_2 captured as CO_3^{2-}. The effects of the chosen parameters were evaluated setting different values of $[CO_3^{2-}]_{in}$ for S, and different values of Q_T. Q_R was set at 30 mL min^{-1} at the beginning and then increased by 10 mL min^{-1} every 12 h until 100 mL min^{-1} was reached. The pH was controlled by adding NaOH and HNO_3 in the stock solutions of K_2CO_3 and $Ca(OH)_2$. The operating pH was monitored using a pH meter/ORP controller PC-310 from Shin Shiang Tech Instruments. The granulation followed the homogeneous granulation process which did not require the addition of seed materials. Sampling was done by collecting two 100 mL water sample from the effluent using 25 mL syringe with one filtered with a 0.45 μm micro-syringe filter. The two samples were then analyzed to calculate the $[Carbonate]_G$, the carbonate fines fraction ($[Carbonate]_{FF}$) and the carbonate granules weight fraction ($[Carbonate]_{WF}$) using Eqs. (5)–(7) respectively. Granulation efficiency and fines fraction were evaluated to determine the percentage of carbonate that formed into granules inside the reactor, fines filtered in effluent, and residues released in effluent.

$$[Carbonate]_G, \% = \left(1 - \frac{[Carbonate]_t \text{ x } Q_T}{\left[CO_3{}^{2-}\right]_{in} \text{ x } Q_{CO_3}}\right) \times 100 \quad (5)$$

$$[Carbonate]_{FF}, \% = \frac{[Carbonate]_f}{\left[CO_3{}^{2-}\right]_{in}} \times 100 \quad (6)$$

$$[Carbonate]_{WF}, \%(\text{every mesh size}) = \frac{W_{ms}}{W_t} \times 100 \quad (7)$$

After every experimental run, the granules formed were collected, air-dried, sieved and analyzed for particle size distribution, surface morphology, molecular structure and elemental composition.

2.4. Analytical methods

The concentrations of dissolved and total effluent carbonate were analyzed using Hach Method 8221 − Phenolphthalein and Total Alkalinity Burette Titration, a standard method for the examination of water and wastewater 2320 B for United States Environmental Protection Agency − National Pollutant Discharge Elimination System (USEPA NPDES). Bicarbonate, carbonate and hydroxide alkalinity were calculated using phenolphthalein and total alkalinity, then bicarbonate and carbonate alkalinity were used as source of final carbonate concentration of dissolved and total effluent carbonate.

The particle size distribution of the granules collected in every operating pH was determined using a sieve analysis, with sieves opening diameters of 2, 1, 0.59, 0.5, 0.42, 0.297 and 0.149 mm. The total weight and the weight in each size fraction were recorded, and these were used in calculating the percentage of each size fraction.

The biggest granules produced after every experiment were collected, dried and sieved for the evaluation of the particle size distribution and for further characterization of the physical and chemical properties. Surface morphology was visualized using Scanning Electron Microscope (SEM, FEI Quanta 200 Environmental Scanning Electron Microscope), granule's structural and molecular formula were determined by X-ray Diffraction (XRD, Multi-function X-ray Diffractometer), and elemental composition was analyzed by Energy Dispersive X-ray (EDX) spectroscopy using same equipment in SEM analysis.

3. Results and discussion

3.1. Influence of supersaturation conditions on $CaCO_3$ granule formation

Calcium carbonate granulation in a fluidized-bed reactor was performed to evaluate the effects of varying S and Q_T on the carbonate ions distribution into granules, fines and residues. The balance equation that governed the nucleation and granulation of $CaCO_3$ in FBR is the double displacement reaction shown in Eqs. (8) and (9), while the degree of supersaturation of the solution with respect to $CaCO_3$ is shown in Eq. (4). Where, $[Ca^{2+}]$ and $[CO_3^{2-}]$ are the activities of calcium and carbonate ions in the solution, respectively, and K_{sp} is the thermodynamic solubility of the $CaCO_3$-aragonite granule which is equal to 6.0×10^{-9}. S values of <1, 1 and >1 represents undersaturation, saturation and oversaturation, respectively (Ramakrishna et al., 2016; Wojtowicz, 2001).

$$K_2CO_3 + Ca(OH)_2 \leftrightharpoons CaCO_3(\text{nuclei}) + 2KOH \quad (8)$$

$$CaCO_3(\text{nuclei}) \leftrightharpoons CaCO_3(\text{granule}) \quad (9)$$

Fig. 2a Illustrates the carbonate end product distribution at different S conditions while maintaining operating pH at 10 ± 0.2, $[Ca^{2+}]/[CO_3^{2-}]$ at 1.50 and Q_T at 60 mL min^{-1}. At S of 10.2, lower granulation efficiency was obtained with average of stable $[Carbonate]_G = 82\%$. This condition achieves an insufficient degree of supersaturation, which resulted in a lower rate of homogeneous nucleation and granulation, which resulted to high carbonate effluent residues. At S of 10.4, efficiency continuously increased to average of stable $[Carbonate]_G = 91\%$ and decreased the carbonate effluent residues. The optimum saturated condition that achieved highest granulation efficiency and lowest carbonate effluent residues was found to be at S of 10.6, with average of stable $[Carbonate]_G = 95\%$. Increasing the concentration of reactant and precipitant provided more ions to react which forms more $CaCO_3$ (De Luna et al., 2015; Pervov, 2015). Higher supersaturation at labile zone increased the granulation rate by overcoming the interfacial tension between the solid and liquid states (Mahasti et al., 2017). Further increasing of the supersaturation in the system by adding more reactant at the same molar ratio caused the reduction of efficiency and increased the carbonate effluent fines and residues. At S of 10.7, the granulation efficiency started to decrease with obtained average of stable $[Carbonate]_G = 92\%$. At S of 10.8, it further proved the downward trend of the efficiency at further increase of S, with average of stable $[Carbonate]_G = 87\%$. Too high supersaturation increased at labile zone favored the severe spontaneous granulation of small fines, which caused the reduction of efficiency and production of sludge. The reactor cannot handle too much chemical loading, which was proven by the increasing carbonate effluent fines and residues at increasing S (Caddarao et al., 2018; Mahasti et al., 2017).

3.2. Effect of influx flow rate on $CaCO_3$ granule formation

Meanwhile Fig. 2b describes the influence of QT on the product distribution. Experiments where conducted maintaining conditions of $[CO_3^{2-}]_{in} = 12$ mM, operating pH at 10 ± 0.2 and $[Ca^{2+}]/[CO_3^{2-}]$ at 1.50. It was observed that lower Q_T yields weaker nucleation because the granulation of $CaCO_3$ in an FBR requires strong collision to form nuclei. Low Q_T results in reduced frequency of collision (Mahasti et al., 2017), which diminishes granulation generation efficiency. At Q_T of 40 mL min^{-1}, it took 120 h to obtain the stable granulation efficiency, with average of stable $[Carbonate]_G = 83\%$. While at Q_T of 50 mL min^{-1}, it took 72 h to obtain the stable efficiency, with average of stable $[Carbonate]_G = 90\%$. The Q_T of 40 and 50 mL min^{-1}, had the lowest fraction of carbonate effluent fines and high carbonate effluent residues. To obtain stable efficiencies at 20 h, Q_T should be set at greater than 60 mL min^{-1}. At Q_T of 60 mL min^{-1}, optimum carbonate granulation efficiency was obtained, with average of stable $[Carbonate]_G = 96\%$. However, further increased of Q_T decreased the granulation efficiency and increased the carbonate effluent fines and residues because too high hydraulic loading allowed the fine particles to reach the effluent region which resulted to easy draining and low granulation efficiency. At Q_T of 70 mL min^{-1}, the granulation efficiency started to decrease proving the above statement, with average of stable $[Carbonate]_G = 91\%$. While at Q_T of 80 mL min^{-1}, the granulation efficiency continued to decrease, with average of stable $[Carbonate]_G = 82\%$.

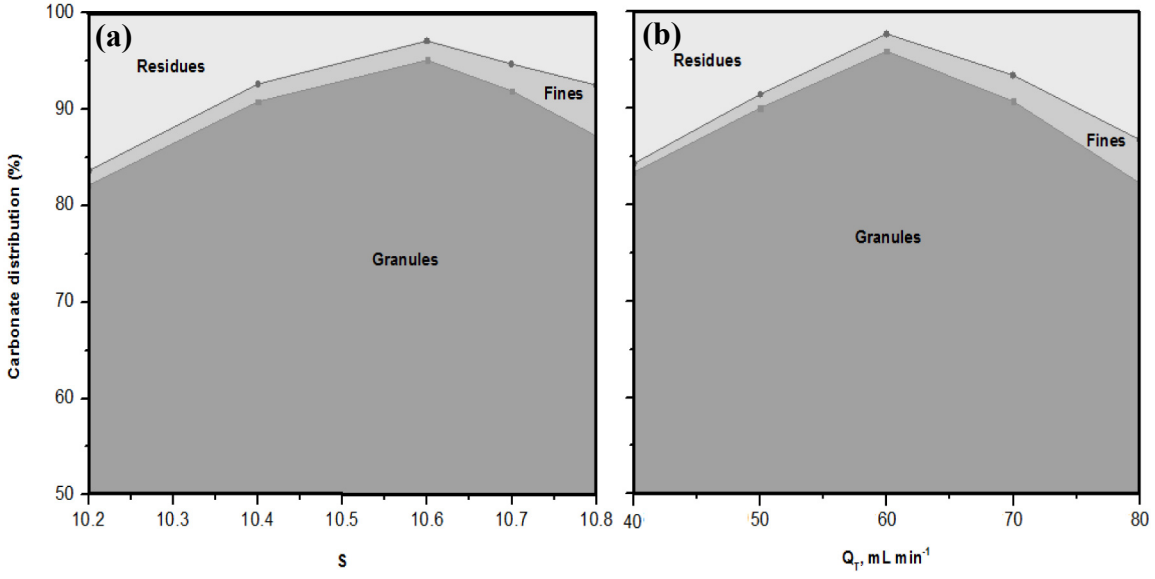

Fig. 2. Effects of varying (a) S and (b) Q_T on carbonate end-product distribution.

3.3. Granule size distribution is defined by supersaturation and flow conditions

Shown in Fig. 3 were the comparisons of the sieve-analyzed particle size distribution trend of $CaCO_3$ granules in every variation of S and Q_T. For S of 10.2, the biggest granule diameter size produced was only 0.5–0.59 mm (Fig. 3a). Starting at S of 10.4 mM, biggest granule diameter size produced were 1–2 mm with ideal particle size distribution trends that shifted toward the production of bigger size granules. Similar to the explanation on the effect of varying S to the carbonate ions end product distribution, higher degree of supersaturation promoted simultaneous homogeneous nucleation and granulation due to high concentration of reactant (Bayon et al., 2019; Petrou and Terzidaki, 2014). At S of 10.6, highest percent weight fraction of 1–2 mm diameter size granules was obtained which was equal to 9%. On this condition, production of smaller granules also started to be observed. Further increase of S, at 10.7 and 10.8, percent weight fraction of 1–2 mm diameter size granules decreased, and production of smaller size granules increased.

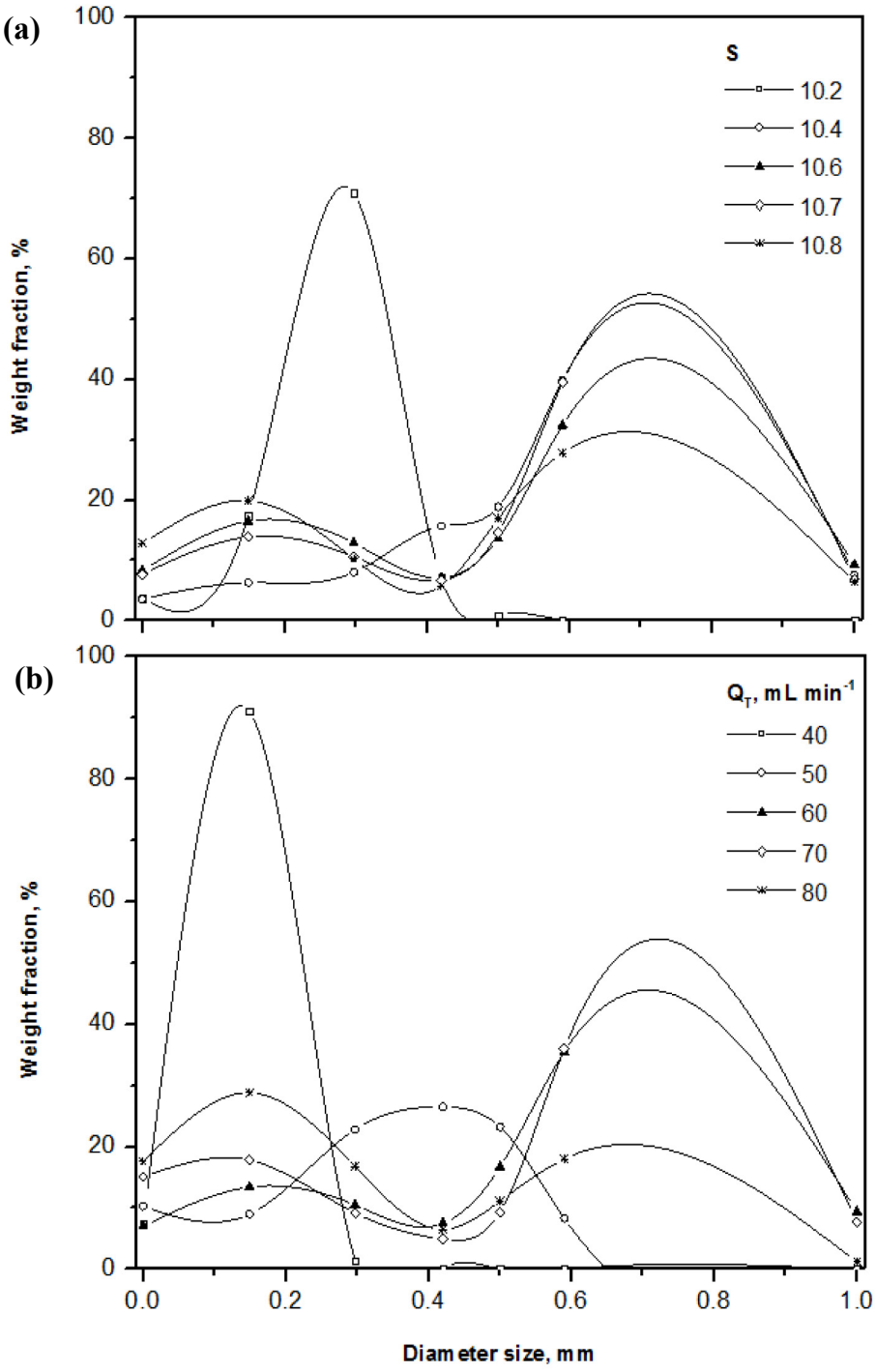

Fig. 3. Particle size distribution trend of granules collected at varying (a) S and (b) Q_T.

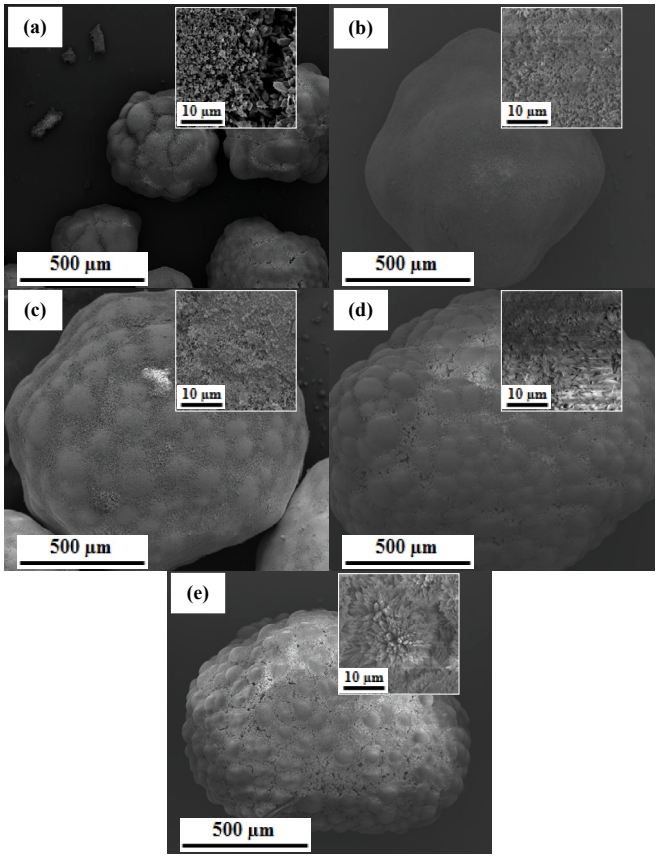

Fig. 4. SEM images showing morphology of $CaCO_3$ granules produced in an FBR at S of (a) 10.2, (b) 10.4, (c) 10.6, (d) 10.7 and (e) 10.8.

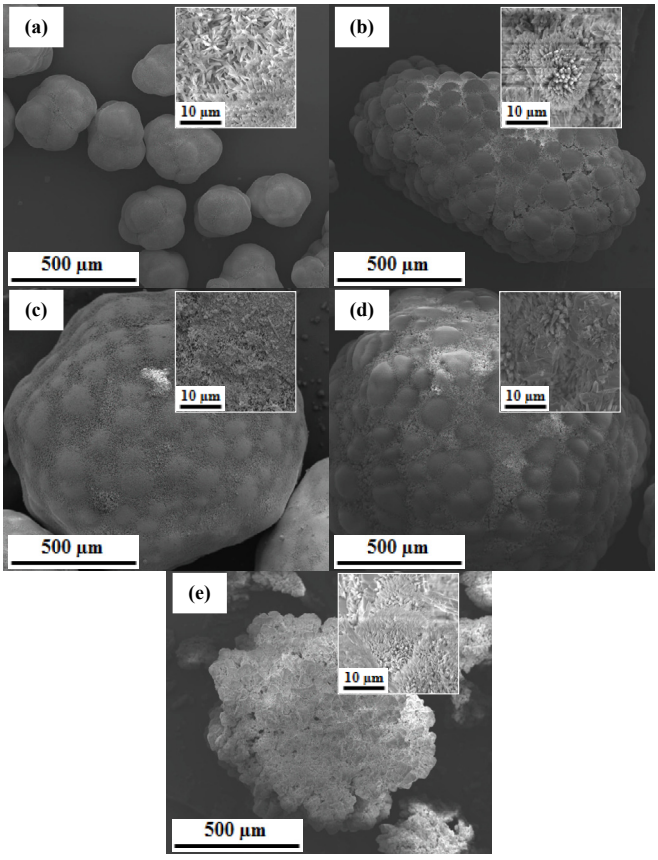

Fig. 5. SEM images showing morphology of $CaCO_3$ granules produced in an FBR at Q_T of (a) 40 mL min^{-1}, (b) 50 mL min^{-1}, (c) 60 mL min^{-1}, (d) 70 mL min-1 and (e) 80 mL min^{-1}.

In Fig. 3b, for Q_T, at 40 mL min^{-1}, the biggest granule diameter size produced was 0.30–0.42 mm. While at Q_T of 50 mL min^{-1}, the biggest granule diameter size produced was 0.59–1.00 mm. Granulation of $CaCO_3$ into particles required strong collision, and very low hydraulic loading reduced the required frequency of collision. Granule diameter size of 1.00–2.00 mm was first observed at Q_T of 60 mL min^{-1}, which also has the highest percent weight fraction equivalent to 10%. This condition also showed favorable particle size distribution trend which is towards the production of bigger granules. As the Q_T continued to increase, at 70–80 mL min^{-1}, percent weight fraction of 1–2 mm diameter size granules decreased, and production of smaller size granules increased. Too high hydraulic loading carried the smaller granules out the effluent before they could agglomerate to form bigger size granules inside the FBR (Mahasti et al., 2017).

Granules of $CaCO_3$ formed inside the reactor through homogeneous nucleation, coagulation-flocculation and granulation mechanisms. The nuclei were formed by chemical bonding of carbonate anions and calcium cations which created smoke like effect inside the reactor. When there were enough number of nuclei present inside the reactor, they coagulate or changes in semisolid state and then clumped to form flocs of $CaCO_3$. Later on, in longer time, the flocs tend to agglomerate to form bigger granules of $CaCO_3$ (Chen et al., 2015; Krossholm, 2012). Fines nucleated in the reactor had the same elemental composition and characteristics than the granules obtained.

3.4. Effects on product characteristics

The physical characteristics of $CaCO_3$ granules produced in FBR in terms of size and surface morphology were checked using SEM analysis, and the SEM images were shown in Figs. 4 and 5 for the results of varying S and Q_T, respectively. The $CaCO_3$ granules produced through homogenous granulation process had the same rounded shapes as shown in 200x magnification, and different exterior surface morphology as revealed by higher magnification of 10,000x magnification (Mahasti et al., 2017; Mohd Abd Ghafar et al., 2017). The nucleus of $CaCO_3$ at early stage formed small rounded particles, and as they grow in number, squeezing between particles inside the reactor became more intense. Thus, allowing the small particles to agglomerate, and with longer retention time to undergo granulation and growth.

As shown in Fig. 4a, at S of 10.2, this condition produced smaller size granules with observed hollows on the surface. Lower supersaturation in terms of chemical loading provided space for the diffusion of particles which prohibited agglomeration and increased the porosity of the granules (Aldaco et al., 2007). At S of 10.4 (Fig. 4b), increasing supersaturation, enough amounts of carbonate and calcium ions were present to precipitate and filled the entire surface which covered the hollows. Both the S of 10.4 and 10.6 had granules with amorphous surface morphology and smaller round particles in the surface (Fig. 4b and c). As the S continuously increased at 10.7 and 10.8, small round particles in the surface also increased in number and size (Fig. 4d and e). Higher S state by increasing chemical loading, the surface morphology of the

granules developed a polymorphic characteristic with crystals growing at the exterior surface as clustered needles (Sommerdijk and With, 2008).

As shown in Fig. 4a, at Q_T of 40 mL min^{-1}, lower Q_T in terms of hydraulic loading produced smaller size granules. At Q_T of 50 mL min^{-1} (Fig. 4b), small round particles in the surface of the granules increased in number and the granules started to grow bigger. Both Q_T of 40 mL min^{-1} and 50 mL min^{-1} produced granules with polymorphic surface. Lower Q_T means lower hydrodynamic force, resulted to granules evolved to crystalline characteristic surface (Mahasti et al., 2017). The hydraulic loading affected the amount of carbon and calcium ions entering the FBR system. Lower Q_T means fewer concentration of carbonate and calcium ions inside the reactor that would nucleate into $CaCO_3$ granule form. The slower homogeneous nucleation occurred inside the reactor at lower Q_T resulted to smaller granule size produced (Abdelaziz et al., 2015). At Q_T of 60 mL min^{-1} (Figs. 4c) and 70 mL min^{-1} (Fig. 4d), the granules produced were bigger and denser with amorphous surface. At Q_T of 80 mL min^{-1} (Fig. 4e), the granules produced started to decrease in size and changes in the exterior surface morphology were started to be observed. Too high Q_T increased the turbulence that induced erosion in the granule surface which inhibited granule growth and increased the number of fine granules in the system (Aldaco et al., 2007).

Larger diameter size of $CaCO_3$ granules were produced in best conditions based on the carbonate ions end product distributions of the parametric experiments varying S and Q_T were collected for analysis of their chemical characteristics. In varying S and Q_T, the optimum conditions were the same which were S = 10.6 ($[CO_3^{2-}]_{in}$ = 12 mM), Q_T = 60 mL min^{-1}, operating pH = 10 ± 0.2 and $[Ca^{2+}]/[CO_3^{2-}]$ = 1.50.

The qualitative analysis of the collected granules was conducted through the XRD test analysis to determine the molecular and structural formula of the granules. As shown in Fig. 6a, the intensity peaks of both optimum conditions were very close to the peaks pattern of $CaCO_3$-aragonite based on JCPDS standard PDF#01-76-0606 (Muryanto et al., 2014). It indicated that the molecular formula of the granules produced was $CaCO_3$ and the structural

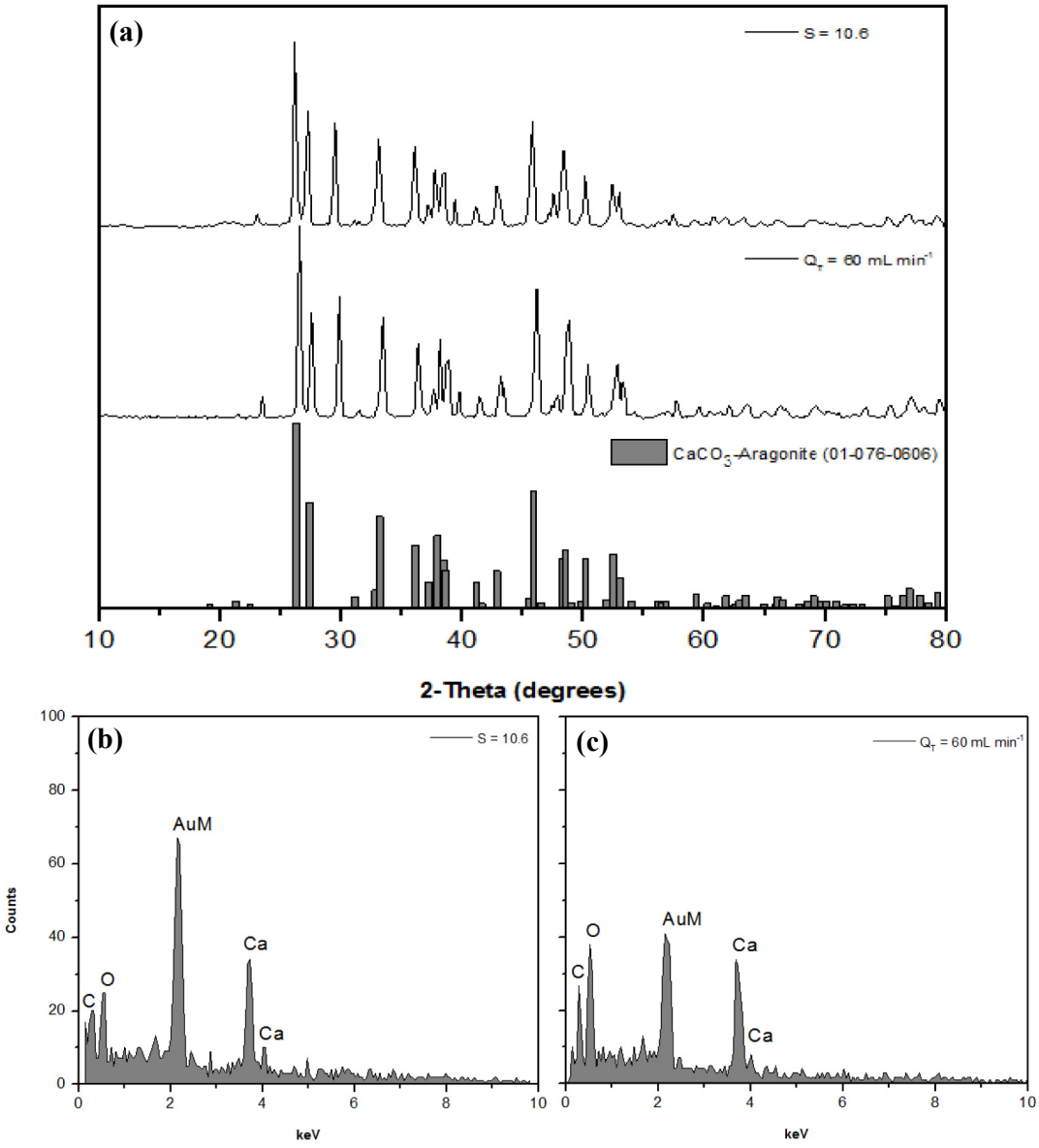

Fig. 6. (a) XRD diagrams, EDX spectra of $CaCO_3$ granules produced at two parametric best conditions of (b) S = 10.6 and (c) Q_T = 60 mL min^{-1}.

arrangement of the atoms conformed to aragonite form. The major peaks under best condition of S of 2-Theta were at 26.2°, 27.3°, 33.1°, 36.1°, 37.7°, 45.8°, 48.4°, 50.1° and 53.0°.While for the Q_T, the major peaks of 2-Theta were at 26.4°, 27.4°, 33.3°, 36.2°, 38.0°, 46.1°, 48.8°, 50.3° and 53.2°. It was reported that longer reaction time increased the intensity peaks of the aragonite diffraction (Ramakrishna et al., 2016). Thus, the 168 h run in every parametric experiment variation correlated to the formation of $CaCO_3$-aragonite in an FBR through the homogeneous granulation process.

The quantitative analysis of the collected granules was done by EDX test analysis to evaluate the elemental composition of the granules. As shown in Fig. 6b and c, it was verified that the produced granules in the best conditions under of S and Q_T were composed of elements C, O and Ca, with no traces of other elements. The $CaCO_3$-aragonite granules produced in a FBR through the homogenous granulation process were of high purity and low moisture content (Mahasti et al., 2017). In addition, the system can be operated in a long-term continuous process. Thus, reduction of CO_2 emission through KOH absorption and $CaCO_3$ granulation possess a great potential and market.

4. Conclusions

The study investigated the effects of the degree of supersaturation and influx flow rate on the $CaCO_3$ homogeneous granulation for CO_2 capture and utilization application. The best operating condition that obtained highest granulation efficiency was found with lowest fractions of carbonate effluent residues and fines, and ideal particle size distribution trend with bigger size granules of up to 1–2 mm in diameter. Optimum S and Q_T conditions were identified as $S = 10.6$ ($[CO_3^{2-}]_{in} = 12$ mM), $Q_T = 60$ mL min^{-1} under operating pH $= 10 \pm 0.2$ and $[Ca^{2+}]/[CO_3^{2-}] = 1.50$. The degree of supersaturation and hydraulic influx flow rate gave significant effect on the surface morphology of the granules collected. At lower S, smaller size granules with hollows on the surface were produced with amorphous surface morphology and smaller round particles. Meanwhile at very high S, the surface morphology of the granules produced have developed a polymorphic characteristic with crystals growing on the exterior surface. Similarly, with lower Q_T, smaller granules with polymorphic surface were produced. Nucleation of $CaCO_3$ requires stronger collision, and very low hydraulic velocity does not provide the required dynamic force to form particles of $CaCO_3$. At higher Q_T, the granules produced started to decrease in size and changes in exterior surface morphology were observed due to surface erosion induced by turbulence at very high hydraulic velocity. These results describe a promising horizon for the revalorization of CO_2 capture solutions by FBHG allowing the production of a commercial by-product during the fixation process. Promising results at this technology readiness level suggest potential competitive application as sustainable technology to control CO_2 emissions. Techno-economic analysis should be conducted in order to evaluate competitiveness and financial viability to identify niche applications while considering conveyance costs. One possible industrial scenario towards cleaner production may consider the use of alkaline industrial effluents as CO_2 saturating solution and fed in the FBHG process. With this approach the FBHG treatment will not only capture CO_2 emitted during a theoretical manufacturing process but will also neutralize the industrial effluent pH (pH $= 6.0–8.0$) as required for additional water treatment or even release.

Declaration of competing interest

The authors declare no competing financial interest.

CRediT authorship contribution statement

Yao-Hui Huang: Conceptualization, Data curation, Formal analysis, Methodology, Visualization. **Sergi Garcia-Segura:** Formal analysis, Supervision, Writing - original draft. **Mark Daniel G. de Luna:** Funding acquisition, Supervision, Validation. **Arianne S. Sioson:** Investigation, Software, Writing - original draft. **Ming-Chun Lu:** Conceptualization, Data curation, Formal analysis, Project administration, Resources, Supervision, Validation.

Acknowledgement

The authors would like to thank the Ministry of Science and Technology, Taiwan (Contract No. MOST-102-2221-E-041-001-MY3) and the Department of Science and Technology, Philippines for providing financial support for this research undertaking.

References

Abdelaziz, M., Ali, A.H., Elbakhshawangy, H.F., Othman, S.H., 2015. Effect of fluid velocity on radioactive ion retention by fluidized-bed reactor. Can. J. Chem. Eng. 93, 905–913. https://doi.org/10.1002/cjce.22182.

Aldaco, R., Garea, A., Irabien, A., 2007. Calcium fluoride recovery from fluoride wastewater in a fluidized bed reactor. Water Res. 41, 810–818. https://doi.org/10.1016/j.watres.2006.11.040.

Bayon, L.L.E., Ballesteros, F.C., Garcia-Segura, S., Lu, M.C., 2019. Water reuse nexus with resource recovery: on the fluidized-bed homogeneous crystallization of copper and phosphate from semiconductor wastewater. J. Clean. Prod. 236, 117705 https://doi.org/10.1016/j.jclepro.2019.117705.

Caddarao, P.S., Garcia-Segura, S., Ballesteros, F.C., Huang, Y.H., Lu, M.C., 2018. Phosphorous recovery by means of fluidized bed homogeneous crystallization of calcium phosphate. Influence of operational variables and electrolytes on brushite homogeneous crystallization. J. Taiwan Inst. Chem. Eng. 83, 124–132. https://doi.org/10.1016/j.jtice.2017.12.009.

Chen, C.S., Shih, Y.J., Huang, Y.H., 2015. Remediation of lead (Pb(II)) wastewater through recovery of lead carbonate in a fluidized-bed homogeneous crystallization (FBHC) system. Chem. Eng. J. 279, 120–128. https://doi.org/10.1016/j.cej.2015.05.013.

Cheng, C.-H., Li, K., Yu, H., Jiang, K., Chen, J., Feron, P., 2018. Amine-based post-combustion CO2 capture mediated by metal ions: advancement of CO2 desorption using copper ions. Appl. Energy 211, 1030–1038. https://doi.org/10.1016/j.apenergy.2017.11.105.

De Luna, M.D.G., Bellotindos, L.M., Asiao, R.N., Lu, M.C., 2015. Removal and recovery of lead in a fluidized-bed reactor by crystallization process. Hydrometallurgy. https://doi.org/10.1016/j.hydromet.2015.03.009.

El-Khouly, M.E., El-Mohsnawy, E., Fukuzumi, S., 2017. Solar energy conversion: from natural to artificial photosynthesis. J. Photochem. Photobiol. C Photochem. Rev. 31, 36–83. https://doi.org/10.1016/j.jphotochemrev.2017.02.001.

Khalilpour, R., Mumford, K., Zhai, H., Abbas, A., Stevens, G., Rubin, E.S., 2015. Membrane-based carbon capture from flue gas: a review. J. Clean. Prod. 103, 286–300. https://doi.org/10.1016/j.jclepro.2014.10.050.

Krossholm, C.K., 2012. Crystal Growth Kinetics of Calcium Carbonate Particles in Natural Gas Production. Norwegian University of Science and Technology (NTNU).

Mahasti, N.N.N., Shih, Y.J., Vu, X.T., Huang, Y.H., 2017. Removal of calcium hardness from solution by fluidized-bed homogeneous crystallization (FBHC) process. J. Taiwan Inst. Chem. Eng. 78, 378–385. https://doi.org/10.1016/j.jtice.2017.06.040.

Medinsky, M. a, 1986. A comparison of ethanolamine and potassium hydroxide as quantitative trapping agents for radiolabeled CO2 in metabolism studies. J. Anal. Toxicol. 10, 24–27.

Minelli, M., Papa, E., Medri, V., Miccio, F., Benito, P., Doghieri, F., Landi, E., 2018. Characterization of novel geopolymer – zeolite composites as solid adsorbents for CO2 capture. Chem. Eng. J. 341, 505–515. https://doi.org/10.1016/j.cej.2018.02.050.

Mohd Abd Ghafar, S.L., Hussein, M.Z., Abu Bakar Zakaria, Z., 2017. Synthesis and characterization of cockle shell-based calcium carbonate aragonite polymorph nanoparticles with surface functionalization. J. Nanoparticles 1–12. https://doi.org/10.1155/2017/8196172, 2017.

Moreira, D., Pires, J.C.M., 2016. Atmospheric CO 2 capture by algae: negative carbon dioxide emission path. Bioresour. Technol. 215, 371–379. https://doi.org/10.1016/j.biortech.2016.03.060.

Mukherjee, A., Okolie, J.A., Abdelrasoul, A., Niu, C., Dalai, A.K., 2019. Review of post-combustion carbon dioxide capture technologies using activated carbon. J. Environ. Sci. (China) 83, 46–63. https://doi.org/10.1016/j.jes.2019.03.014.

Muryanto, S., Bayuseno, A.P., Ma'mun, H., Usamah, M., Jotho, 2014. Calcium carbonate scale formation in pipes: effect of flow rates, temperature, and malic acid as additives on the mass and morphology of the scale. Procedia Chem 9, 69–76. https://doi.org/10.1016/j.proche.2014.05.009.

Patricio, J., Angelis-Dimakis, A., Castillo-Castillo, A., Kalmykova, Y., Rosado, L., 2017. Region prioritization for the development of carbon capture and utilization technologies. J. CO2 Util. 17, 50–59. https://doi.org/10.1016/j.jcou.2016.10.002.

Pervov, A.G., 2015. Precipitation of calcium carbonate in reverse osmosis retentate flow by means of seeded techniques — a tool to increase recovery. Desalination 368, 140–151. https://doi.org/10.1016/j.desal.2015.02.024.

Petrou, A.L., Terzidaki, A., 2014. Calcium carbonate and calcium sulfate precipitation, crystallization and dissolution: evidence for the activated steps and the mechanisms from the enthalpy and entropy of activation values. Chem. Geol. 381, 144–153. https://doi.org/10.1016/j.chemgeo.2014.05.018.

Ramakrishna, C., Thenepalli, T., Huh, J.H., Ahn, J.W., 2016. Preparation of needle like aragonite precipitated calcium carbonate (PCC) from dolomite by carbonation method. J. Korean Ceram. Soc. 53, 7–12. https://doi.org/10.4191/kcers.2016.53.1.7.

Salcedo, A.F.M., Ballesteros, F.C., Vilando, A.C., Lu, M.C., 2016. Nickel recovery from synthetic Watts bath electroplating wastewater by homogeneous fluidized bed granulation process. Separ. Purif. Technol. 169, 128–136. https://doi.org/10.1016/j.seppur.2016.06.010.

Sánchez-Sánchez, C.M., Souza-Garcia, J., Herrero, E., Aldaz, A., 2012. Electrocatalytic reduction of carbon dioxide on platinum single crystal electrodes modified with adsorbed adatoms. J. Electroanal. Chem. 668, 51–59. https://doi.org/10.1016/j.jelechem.2011.11.002.

Sharma, N., 2018. Silver bullet or bitter pill? Reassessing the scope of CO2 capture and storage in India. Carbon Manag. 9, 311–332. https://doi.org/10.1080/17583004.2018.1518108.

Singh, J., Bhunia, H., Basu, S., 2018. CO2adsorption on oxygen enriched porous carbon monoliths: kinetics, isotherm and thermodynamic studies. J. Ind. Eng. Chem. 60, 321–332. https://doi.org/10.1016/j.jiec.2017.11.018.

Smirnova, N., Demyan, M.S., Rasche, F., Cadisch, G., Müller, T., 2014. Calibration of CO2 trapping in alkaline solutions during soil incubation at varying temperatures using a respicond VI. Open J. Soil Sci. 4, 161–167. https://doi.org/10.4236/ojss.2014.45019.

Sommerdijk, N. a J.M., With, G. De, 2008. Biomimetic CaCO3 mineralization using designer molecules and interfaces. Chem. Rev. 108, 4499–4550. https://doi.org/10.1021/cr078259o.

Thompson, J.G., Matin, N.S., Abad, K., Onneweer, F., Bhatnagar, S., 2018. Determining the Henry's volatility coefficient of nitrosamines in CO2 capture solvents. Int. J. Greenh. Gas Control 73, 104–110. https://doi.org/10.1016/j.ijggc.2018.04.004.

Wang, T., Hovland, J., Jens, K.J., 2015. Amine reclaiming technologies in post-combustion carbon dioxide capture. J. Environ. Sci. (China) 27, 276–289. https://doi.org/10.1016/j.jes.2014.06.037.

Wojtowicz, J.A., 2001. Calcium carbonate precipitation potential. J. Swim. Pool Spa Ind. 2, 51–57.

Yoo, M.-R., Han, S.-J., Shin, J.-Y., Wee, J.-H., 2012. A study on carbon dioxide capture performance of KOH aqueous solution via chemical absorption. J. Korean Soc. Environ. Eng. 34, 55–62. https://doi.org/10.4491/KSEE.2012.34.1.055.

Zhang, F., Zhang, H., Liu, Z., 2019. Recent advances in electrochemical reduction of CO2. Curr. Opin. Green Sustain. Chem. 16, 77–84. https://doi.org/10.1016/j.cogsc.2019.02.006.

Zhang, Z., Huisingh, D., 2017. Carbon dioxide storage schemes : technology , assessment and. J. Clean. Prod. 142, 1055–1064. https://doi.org/10.1016/j.jclepro.2016.06.199.